



## Effect of Mg–Nb oxides addition on hydrogen sorption in MgH<sub>2</sub>

M.W. Rahman<sup>a</sup>, A. Castellero<sup>a</sup>, S. Enzo<sup>b</sup>, S. Livraghi<sup>a</sup>, E. Giamello<sup>a</sup>, M. Baricco<sup>a,\*</sup>

<sup>a</sup> Dipartimento di Chimica IFM, NIS Centre of Excellence, Università di Torino, Via Pietro Giuria 9, 10125 Torino, Italy

<sup>b</sup> Dipartimento di Chimica, Università di Sassari, 07100 Sassari, Italy

### ARTICLE INFO

#### Article history:

Received 4 July 2010

Received in revised form 6 February 2011

Accepted 13 February 2011

Available online 24 February 2011

#### Keywords:

Hydrogen storage materials

High-energy ball milling

X-ray diffraction

### ABSTRACT

H<sub>2</sub> absorption and desorption reactions in MgH<sub>2</sub> promoted by ball-milling with 1 mol% MgNb<sub>2</sub>O<sub>6</sub>, Mg<sub>4</sub>Nb<sub>2</sub>O<sub>9</sub> and Mg<sub>3</sub>Nb<sub>6</sub>O<sub>11</sub> have been investigated. MgH<sub>2</sub> was milled with the bare oxides for 12 h under a high purity Ar atmosphere. Absorption and desorption reactions in the ball-milled samples were studied by in situ X-ray diffraction (XRD) in isothermal conditions with Anton Paar XRD 900 reaction chamber. XRD patterns for absorption were recorded at 573 K under hydrogen pressure of 0.9 MPa and for desorption at 623 K in vacuum. Experimental data were analysed according to the Rietveld method. Ball-milled samples showed the presence of a mixture of β and γ allotropes of MgH<sub>2</sub>, with significantly broadened diffraction peaks due to reduced crystallite size and strain, together with bare additives. The presence of Mg–Nb oxides significantly accelerates the hydrogen absorption and desorption processes. The amount of hydrogen absorbed in the presence of Mg–Nb–O phases is lower than the maximum stoichiometric capacity, because of the presence of a non-reactive MgO layer on the surface of the powders or at the grain boundaries. Experimental results are discussed on the basis of thermodynamic and kinetic arguments.

© 2011 Elsevier B.V. All rights reserved.

### 1. Introduction

Magnesium hydride is considered a promising hydrogen storage material because of a high nominal H<sub>2</sub> storage capacity (7.6 wt%). However, the reaction kinetics of hydrogen absorption and desorption is too slow in moderate conditions. Ball milling of pure MgH<sub>2</sub> was reported to increase significantly the absorption and desorption reaction rates [1]. Kinetic parameters seem to be related to particle size distribution [2] and to the presence of impurities [3]. It was reported that milling MgH<sub>2</sub> with various additives leads to a significant improvement in the reaction kinetics [4]. In particular, Nb<sub>2</sub>O<sub>5</sub> addition showed a remarkable effect on kinetics during the hydrogen sorption cycles [5–10]. Explanations for these improvements of the reaction kinetics have been suggested on the basis of mechanical effects of the oxide particles on MgH<sub>2</sub> grain refinement during ball milling [4,6] or on a pinning effect, limiting the grain growth during reactions [11]. On the other hand, chemical effects on MgH<sub>2</sub> of the additive have been also considered [5–7]. A destabilization of the magnesium hydride by the oxide, leading to a MgH<sub>2-δ</sub> phase, has been suggested as a result of the interaction of the additive with the MgO layer surrounding the Mg particles [12]. The reaction kinetic improvement has been also explained by the formation of ternary Mg–Nb–O phases [6–9]. On the basis of a careful X-ray photoelectron spectroscopy and transmission electron

microscopy analysis, the evidence of a reduction on the oxidation state of Nb in the oxide phase has been suggested and a reactive pathway model, where Nb<sub>2</sub>O<sub>5</sub> is reduced to metallic Nb, together with a simultaneous formation of ternary Mg–Nb–O phases of various stoichiometry at the interface with the MgH<sub>2</sub> phase, has been proposed to facilitate hydrogen diffusion [7].

In order to understand the specific role of Mg–Nb oxides on the hydrogen sorption reactions in MgH<sub>2</sub>, specific studies on the hydrogen interactions with the bare additives have been carried out. The interaction of hydrogen with bare Nb<sub>2</sub>O<sub>5</sub> (and other oxides such as WO<sub>3</sub>) was first investigated [13,14]. This was done to connect the kinetic activity of these promoters to their propensity to include hydrogen and form typical intercalation compounds called bronzes. A preliminary study on reversible hydrogen uptake properties of binary and ternary Mg–Nb–O compounds, suggested that Mg<sub>3</sub>Nb<sub>6</sub>O<sub>11</sub> has a significant reactivity with hydrogen [15,16]. On the other hand, a specific investigation on the role of ternary Mg–Nb oxide addition to MgH<sub>2</sub> during ball milling on the hydrogen sorption kinetics is still lacking.

In this work, H<sub>2</sub> sorption and desorption reactions in MgH<sub>2</sub> promoted by ball-milling with 1 mol% MgNb<sub>2</sub>O<sub>6</sub>, Mg<sub>4</sub>Nb<sub>2</sub>O<sub>9</sub> and Mg<sub>3</sub>Nb<sub>6</sub>O<sub>11</sub> will be investigated. Milled pure MgH<sub>2</sub> and MgH<sub>2</sub>–Nb<sub>2</sub>O<sub>5</sub> mixtures were taken as reference materials. In situ X-ray diffraction (XRD) has been shown to be a suitable tool for the study of the effect of additives on hydrogen sorption kinetics in Mg [17]. So, in this paper, the sorption reactions will be studied by in situ XRD, with the aim to follow the relative amount of the various phases in the mixture as a function of time. Experimental

\* Corresponding author. Tel.: +39 011 670 7569; fax: +39 011 670 7855.  
E-mail address: [marcello.baricco@unito.it](mailto:marcello.baricco@unito.it) (M. Baricco).

results will be discussed on the basis of the effects of the nanostructured  $\text{MgH}_2$  and of the additive on the thermodynamics and kinetics of the hydrogen sorption reactions.

## 2. Experimental

The starting materials used for solid-state synthesis of ternary oxides were commercially available magnesium oxide ( $\text{MgO}$ ), niobium (V) oxide ( $\text{Nb}_2\text{O}_5$ ) and metallic niobium ( $\text{Nb}$ ). Three Mg–Nb–O compounds were synthesized by calcination of the parent materials for 24 h at different temperatures, ranging from 873 to 1473 K. Annealing temperatures were reached from room temperature (RT) with heating rate of 5 K/min.  $\text{MgNb}_2\text{O}_6$  and  $\text{Mg}_4\text{Nb}_2\text{O}_9$  were prepared by heating the  $\text{MgO}/\text{Nb}_2\text{O}_5$  precursors in the correct molar ratio in air.  $\text{Mg}_3\text{Nb}_6\text{O}_{11}$  was prepared in evacuated quartz ampoules.

1 mol% of oxide was added to 5 g of commercial  $\text{MgH}_2$ . Mechanical treatments were performed in a commercial Spex Mod-8000 Mixer-Mill for 12 h under a high purity Ar atmosphere. The milling runs were carried out at 875 rpm by employing a special hardened steel vial and two hardened steel milling balls with a ball-to-powder ratio of 7:1. Ball milled mixtures with the various oxides will be named on the basis of the additives:  $\text{Nb}_2\text{O}_5$  ( $\text{O}_5$ ),  $\text{MgNb}_2\text{O}_6$  ( $\text{O}_6$ ),  $\text{Mg}_4\text{Nb}_2\text{O}_9$  ( $\text{O}_9$ ) and  $\text{Mg}_3\text{Nb}_6\text{O}_{11}$  ( $\text{O}_{11}$ ). Ball milled pure  $\text{MgH}_2$  was taken as a reference (BM).

The structure of as-prepared materials has been analysed by XRD at room temperature with an X-Pert diffractometer (Panalytical) with  $\text{Cu K}\alpha$  radiation. In situ XRD was performed using a hot stage and environmental chamber (Anton Paar XRK 900). XRD patterns were collected in a  $0.017^\circ$  step for 6 min, with suitable temperature step programs. For desorption experiments, after heating from room temperature up to 623 K at 20 K/min under 0.9 MPa of  $\text{H}_2$  pressure, a continuous rotary vacuum was introduced in the chamber and XRD diffraction patterns were recorded as function of time for 10 h. For absorption experiments, after heating from room temperature up to 673 K at 20 K/min under 0.9 MPa of  $\text{H}_2$  pressure, a continuous rotary vacuum was introduced in the chamber for 15 h in order to complete the desorption reaction in the sample. After cooling down to 573 K, a constant pressure of 0.9 MPa of  $\text{H}_2$  was introduced in the chamber and XRD diffraction patterns were recorded as function of time for 15 h.

Assessment of structural information contained in the powder XRD patterns was made using MAUD (Material Analysis Using Diffraction), a general diffraction/reflectivity analysis program mainly based on the Rietveld method and oriented to materials science studies [18].

## 3. Results

The XRD patterns of as-prepared ternary oxides are shown in Fig. 1 (patterns a–c). After the synthesis, pure compounds have been obtained. The grain size is rather big in all cases, as evidenced by the doublet splitting in the diffraction peaks. Ball milling of  $\text{MgH}_2$  leads to a microstructure refinement, as shown in Fig. 1 (pattern d). Together with the presence of parent  $\beta$ -tetragonal  $\text{MgH}_2$ , the formation of a small amount of  $\gamma$ -orthorhombic  $\text{MgH}_2$  is observed. This phase is stable at high pressure and its formation is often promoted by ball milling [2]. In addition, a significant amount of  $\text{MgO}$  phase (lower than 10 wt%) is also obtained, because of possible Mg oxidation during the milling process. After ball milling with  $\text{MgH}_2$ , a significant broadening of diffraction peaks of additives is evidenced in the XRD patterns, as shown in Fig. 1 (patterns e–h). The crystallite size of the additives becomes lower than 100 nm, but it never reaches that of  $\text{MgH}_2$  (around 10 nm). A detailed description of phase constitution, lattice constants and microstructural parameters for as milled samples is reported in Table 1, as obtained from Rietveld refinement with a  $R\%$  of about 7–9%. In all cases, after ball milling, the lattice constants of  $\beta$ - $\text{MgH}_2$  are very similar to those measured on as-received materials and those reported in the crystallographic database (ICSD-01-074-0934,  $a_0 = 4.5168 \text{ \AA}$  and  $c_0 = 3.0205 \text{ \AA}$ ). On the basis of the 1 mol% addition, the theoretical phase fraction of the additive for the various mixtures is equal to 9.2 wt%, 10.5 wt%, 14.1 wt% and 23.6 wt% for the  $\text{O}_5$ ,  $\text{O}_6$ ,  $\text{O}_9$  and  $\text{O}_{11}$  samples, respectively. From the results of the Rietveld analysis (Table 1), it turns out that during ball milling the relative amount of additive remains basically unchanged, suggesting no interaction with  $\text{MgH}_2$ .

The results of the in situ experiment of hydrogen desorption at 623 K are reported in Fig. 2. For each sample, three patterns are shown, corresponding to the beginning (bottom pattern, 3 min),

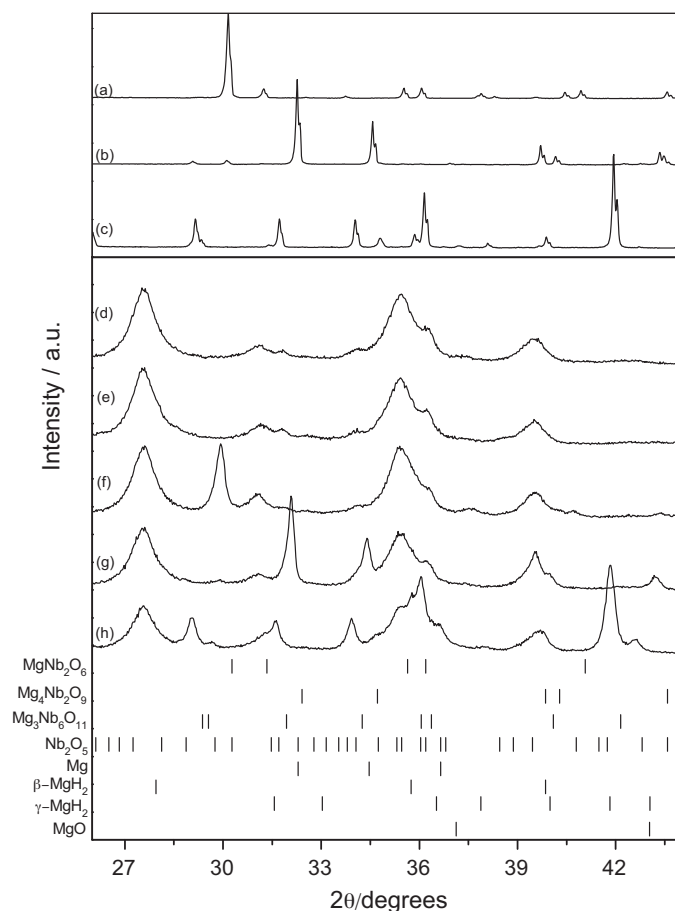


Fig. 1. XRD patterns taken at room temperature for (a)  $\text{MgNb}_2\text{O}_6$ , (b)  $\text{Mg}_4\text{Nb}_2\text{O}_9$ , (c)  $\text{Mg}_3\text{Nb}_6\text{O}_{11}$ , (d) ball milled  $\text{MgH}_2$ , (e)  $\text{O}_5$ , (f)  $\text{O}_6$ , (g)  $\text{O}_9$  and (h)  $\text{O}_{11}$  ball milled mixtures.

the middle (middle pattern, 250 min) and the end (top pattern, 990 min) of the reaction. The phase evolution is well evident, with the diffraction peaks of  $\text{MgH}_2$  progressively decreasing as a function of the annealing time, together with a continuous increase of the diffraction peaks of Mg. A significant grain refinement occurs for  $\text{MgH}_2$ , which reaches a crystallite size of about 50–60 nm during the heating from room temperature to the annealing temperature. A significant shift (about  $0.5^\circ$ ) of diffraction peaks is observed in the XRD patterns measured at 623 K (Fig. 2) with respect to those obtained at room temperature (Fig. 1). It seems to increase during the isothermal treatment, as well evidenced by the position of the diffraction peaks of the  $\text{MgH}_2$  phase at different annealing times. The thermal expansion of the ceramic sample holder has been estimated with a sample of pure Ni, and it brings to an angle shift of less than  $0.1^\circ$ . On the other hand, the observed peak shift cannot account for the thermal expansion of the crystalline phases, which would bring to a limited variation of the lattice constants. So, it is considered that during desorption, the powdered sample surface moves significantly from the centre of the goniometer, because of the volume variation due to hydrogen desorption. In the case of mixtures with ternary oxides, the presence of the additive is well evident also at 623 K. On the contrary, when  $\text{Nb}_2\text{O}_5$  is added, only the diffraction peaks of Mg and  $\text{MgH}_2$  phases are clearly evidenced.

The XRD patterns obtained during the in situ absorption experiments at 573 K are reported in Fig. 3. For each sample, the pattern obtained after desorption in vacuum at 673 K and before  $\text{H}_2$  insertion in the reaction chamber is reported for reference (top pattern). During the experiment, the intensity of the  $\text{MgH}_2$  diffraction peaks increase because of hydrogen absorption, together with the simul-

**Table 1**  
Crystallographic parameters extracted from Rietveld analysis of XRD patterns of as-received, ball-milled  $\text{MgH}_2$ ,  $\text{MgH}_2 + \text{Nb}_2\text{O}_5$ ,  $\text{MgH}_2 + \text{MgNb}_2\text{O}_6$ ,  $\text{MgH}_2 + \text{Mg}_4\text{Nb}_2\text{O}_9$  and  $\text{MgH}_2 + \text{Mg}_3\text{Nb}_6\text{O}_{11}$  measured at room temperature.

Sample	Phase	Wt%	Lattice constants (Å)			Crystallite size (nm)	Microstrain	R%
			a	b	c			
MgH <sub>2</sub> as received	β-MgH <sub>2</sub>	93	4.519	–	3.022	220	5.7E–4	9.0
	Mg	7	3.213	–	5.218	250	1.0E–3	
MgH <sub>2</sub> ball milled	β-MgH <sub>2</sub>	70	4.513	–	3.021	10	1.9E–3	7.0
	γ-MgH <sub>2</sub>	16	4.505	5.420	4.916	15	8.0E–4	
	Mg	5	3.213	–	5.232	20	1.0E–3	
	MgO	9	4.229	–	–	4	8.0E–4	
	MgH <sub>2</sub> + Nb <sub>2</sub> O <sub>5</sub> ball milled	β-MgH <sub>2</sub>	72	4.516	–	3.019	11	
γ-MgH <sub>2</sub>	9	4.505	5.412	4.917	25	8.0E–4		
Mg	5	3.213	–	5.211	30	1.0E–3		
MgO	5	4.217	–	–	4	8.0E–4		
Nb <sub>2</sub> O <sub>5</sub>	9	21.204	3.823	19.338	25	1.3E–3		
MgH <sub>2</sub> + MgNb <sub>2</sub> O <sub>6</sub> ball milled	β-MgH <sub>2</sub>	70	4.517	–	3.020	10	2.0E–4	6.9
	γ-MgH <sub>2</sub>	5	4.517	5.426	4.916	20	8.0E–4	
	Mg	7	3.248	–	5.237	15	1.0E–3	
	MgO	5	4.228	–	–	6	8.0E–4	
	MgNb <sub>2</sub> O <sub>6</sub>	13	14.194	5.703	5.039	30	3.7E–4	
	MgH <sub>2</sub> + Mg <sub>4</sub> Nb <sub>2</sub> O <sub>9</sub> ball milled	β-MgH <sub>2</sub>	69	4.513	–	3.019	10	
γ-MgH <sub>2</sub>	5	4.524	5.415	4.934	20	8.0E–4		
Mg	5	3.228	–	5.206	20	1.0E–3		
MgO	5	4.187	–	–	6	8.0E–4		
Mg <sub>4</sub> Nb <sub>2</sub> O <sub>9</sub>	16	5.163	–	14.027	80	9.6E–4		
MgH <sub>2</sub> + Mg <sub>3</sub> Nb <sub>6</sub> O <sub>11</sub> ball milled	β-MgH <sub>2</sub>	58	4.515	–	3.020	10	2.3E–4	7.9
	γ-MgH <sub>2</sub>	15	4.495	5.557	4.907	70	1.0E–3	
	MgO	3	4.217	–	–	25	8.0E–4	
	Mg <sub>3</sub> Nb <sub>6</sub> O <sub>11</sub>	24	6.038	–	7.463	45	1.1E–3	

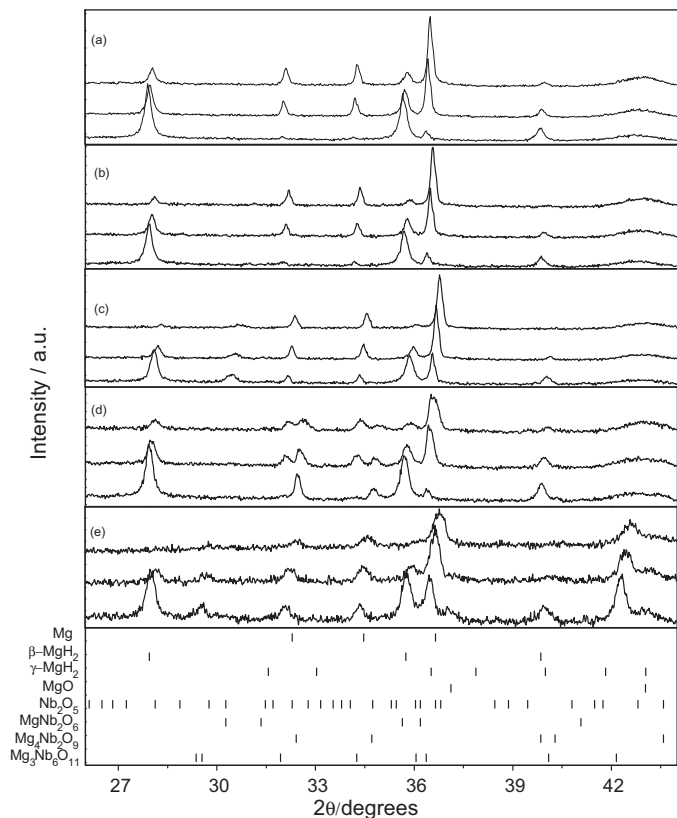


**Fig. 2.** In situ XRD patterns for H<sub>2</sub> desorption under vacuum at 623 K for (a) ball milled  $\text{MgH}_2$ , (b) O<sub>5</sub>, (c) O<sub>6</sub>, (d) O<sub>9</sub> and (e) O<sub>11</sub> ball milled mixtures. For each sample, three patterns are shown, corresponding to (bottom pattern) 3 min, (middle pattern) 250 min and (top pattern) 990 min of annealing.

taneous decrease of the diffraction peaks of the Mg phase, as shown in Fig. 3 for XRD patterns collected after 3 min (middle pattern) and 300 min (bottom pattern). A part for the BM mixture, in all

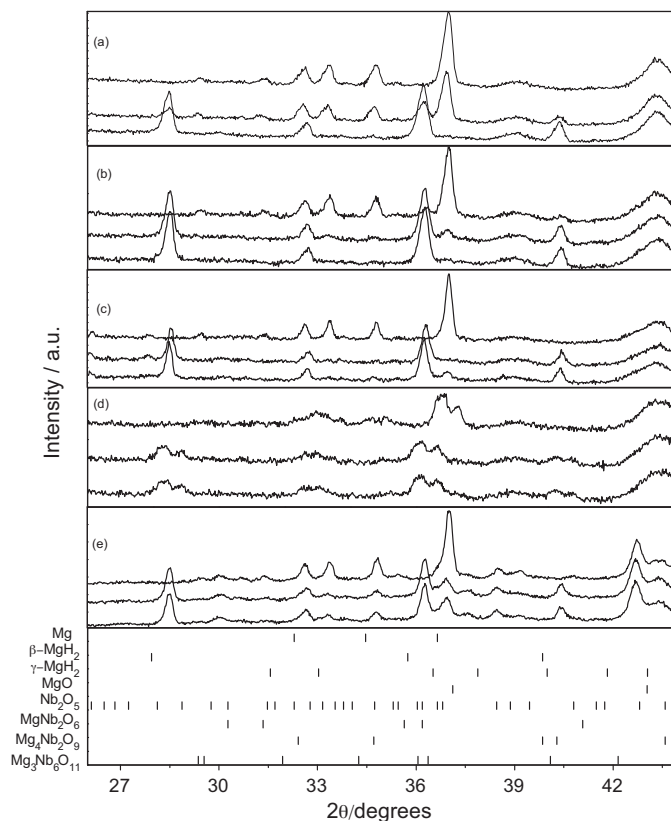


**Fig. 3.** In situ XRD patterns for H<sub>2</sub> absorption at 573 K for (a) ball milled  $\text{MgH}_2$ , (b) O<sub>5</sub>, (c) O<sub>6</sub>, (d) O<sub>9</sub> and (e) O<sub>11</sub> ball milled mixtures. For each sample, three patterns are shown, corresponding to vacuum condition (top pattern), 3 min (middle pattern) and 300 min (bottom pattern) under 0.9 MPa of H<sub>2</sub> pressure.

the cases after 3 min of reaction, a significant H<sub>2</sub> absorption is already observed, suggesting a significant role of additives also on the rate of absorption reaction. Also in this case, a significant shift

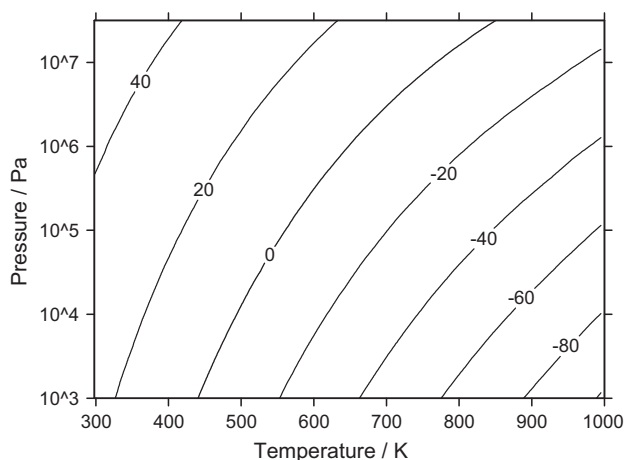


Fig. 4. Calculated driving forces for hydrogen absorption/desorption in Mg as a function of temperature and pressure. Lines connect constant values in  $\text{kJ mol}^{-1}_{\text{H}_2}$ .

of the diffraction peaks with respect to the theoretical position is observed, likely because of the volume variation during absorption.

#### 4. Discussion

In order to estimate the thermodynamic and kinetic effects of hydrogen absorption and desorption in  $\text{MgH}_2$  with various additives, a thermodynamic analysis of the phase transformation has been carried out. In particular, from available thermodynamic databases [19], the driving forces for hydrogen absorption and desorption in Mg have been calculated according to the reaction:



The results are reported in Fig. 4, where lines connecting constant values of free energy difference for reaction (1) are reported as a function of pressure and temperature. It turns out that, for a constant pressure of 0.9 MPa, a driving force of about  $10 \text{ kJ mol}^{-1}_{\text{H}_2}$  is acting at 573 K for the absorption reaction. On the other hand, for the desorption reaction at 623 K, the driving force strongly depends on the actual  $\text{H}_2$  partial pressure in the chamber. If a value of about  $10^{-2}$  MPa is considered, a much higher driving force for the reaction is estimated. As a consequence, on the basis of thermodynamic arguments, a faster reaction would be expected for desorption with respect to absorption. It is worth to note that, for the absorption reactions at constant pressure, an increase of the temperature will reduce significantly the driving force. As a consequence, the beneficial effects on the kinetics of the reaction due to a higher diffusion coefficient, can be slowed down for absorption processes at high temperatures.

The presence of nanostructured materials may have significant effects on the thermodynamics and kinetics of the hydrogenation/dehydrogenation reaction [19]. The presence of free surfaces will affect the free energy of both Mg and  $\text{MgH}_2$  phases, according to the Gibbs–Thompson effect [20]. In standard conditions, the free energy change ( $\Delta G$ ) of reaction (1) due to the presence of particles with radius ( $r$ ) will be given by [21]:

$$\Delta G(r) = \frac{3V_{\text{Mg}} \left[ \gamma_{\text{MgH}_2} (V_{\text{MgH}_2}/V_{\text{Mg}})^{2/3} - \gamma_{\text{Mg}} \right]}{r} \quad (2)$$

where  $V_{\text{Mg}}$  and  $V_{\text{MgH}_2}$  are the molar volumes and  $\gamma_{\text{Mg}}$  and  $\gamma_{\text{MgH}_2}$  are the surface energies of the Mg and  $\text{MgH}_2$  phases, respectively. As a consequence, at standard  $p_{\text{H}_2}^{\text{eq}} = 1 \text{ bar}$ , the variation in the decomposition temperature ( $\Delta T_{\text{dec}}$ ) can be calculated according

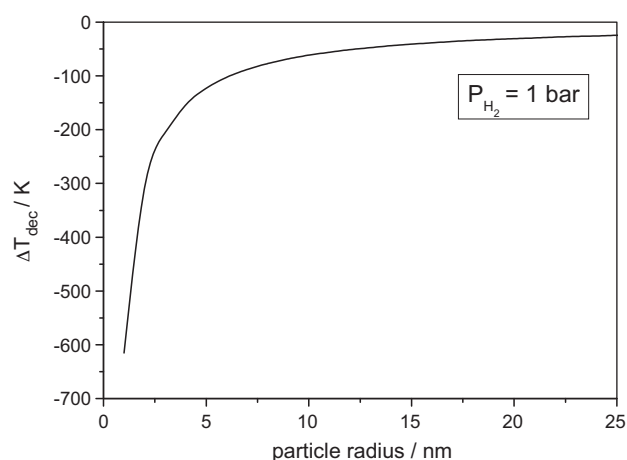


Fig. 5. Variation of equilibrium decomposition temperature for hydrogen absorption/desorption in Mg as a function of the particle radius, according to Eq. (3).

to:

$$\Delta T_{\text{dec}} = \frac{3V_{\text{Mg}} \left[ \gamma_{\text{MgH}_2} (V_{\text{MgH}_2}/V_{\text{Mg}})^{2/3} - \gamma_{\text{Mg}} \right]}{\Delta S_0 r} \quad (3)$$

where  $\Delta S_0$  is the standard entropy for reaction (1). An estimation of the effect of free surface on the decomposition temperature for the Mg/ $\text{MgH}_2$  reaction has been obtained with [21,22]:  $\Delta S_0 = -130 \text{ J mol}^{-1}_{\text{H}_2} \text{ K}^{-1}$ ,  $V_{\text{Mg}} = 1.38 \times 10^{-5} \text{ m}^3 \text{ mol}^{-1}$ ,  $V_{\text{MgH}_2} = 1.81 \times 10^{-5} \text{ m}^3 \text{ mol}^{-1}$ ,  $\gamma_{\text{Mg}} = 0.55 \text{ J m}^{-2}$  and  $\gamma_{\text{MgH}_2} = 2.08 \text{ J m}^{-2}$ . The results are shown in Fig. 5, where the decrease of  $T_{\text{dec}}$  at 1 bar is reported as a function of the particle radius. It is clear that, if a  $T_{\text{dec}} = 577 \text{ K}$  is considered for the bulk sample, corresponding to a standard enthalpy for reaction (1),  $\Delta H_0 = -75 \text{ kJ mol}^{-1}_{\text{H}_2}$ , a crystallite size of about 2.3 nm would be necessary to bring the decomposition temperature close to room temperature. This stabilisation effects have been recently estimated for Mg clusters by ab-initio calculations, suggesting a decrease of  $T_{\text{dec}}$  of more than 100 K for particle sizes of the order of 1.3 nm [23]. Such a small values of particle size can be hardly obtained, even by ball milling or inert gas condensation [2,10,24]. In addition, it is to consider that, in real systems, free standing surfaces will be strongly reduced by adhesion and surface reconstruction, so that surface energies should be replaced by grain boundaries energies ( $\gamma_{\text{gb}}$ ) [21]. On the other hand, the presence of a hydrogen pressure in the grain boundaries, might modify the values of  $\gamma_{\text{gb}}$ . Of course, the presence of combined parameters in  $\Delta G(r)$  (Eq. (2)) might also brings to destabilisation effects in  $\text{H}_2$  sorption reactions. In fact, a reduction of particle size might lead to more negative values of  $\Delta H_0$ , as recently demonstrated with ab-initio calculations [25]. As an example, a reduction of particle size for the Ti/ $\text{TiH}_2$  reaction brings to an increase of  $T_{\text{dec}}$ . Of course, this effect might be useful for unstable hydrides (e.g.,  $\text{AlH}_3$ ) that might become stable with a significant reduction of the particle size.

From the analysis of possible effects of a nanostructured material on the thermodynamics of hydrogenation/dehydrogenation reaction, the occurrence of an excess volume ( $V_{\text{exc}}$ ) plays the major role. In particular, the presence of moderate strained region in the material leads to a reduction of  $T_{\text{dec}}$  if [21]:

$$V_{\text{MgH}_2} B_{0,\text{MgH}_2} > V_{\text{Mg}} B_{0,\text{Mg}} \quad (4)$$

where  $B_{0,\text{Mg}}$  and  $B_{0,\text{MgH}_2}$  are the bulk modulus of the Mg and  $\text{MgH}_2$  phases, respectively. If  $B_{0,\text{Mg}} = 45 \text{ GPa}$  and  $B_{0,\text{MgH}_2} = 55 \text{ GPa}$  are considered [22], it turns out that a decrease of  $T_{\text{dec}}$  can be obtained, as recently demonstrated for absorption experiments in thin films [26]. Even in this case, different elastic properties for the metal and

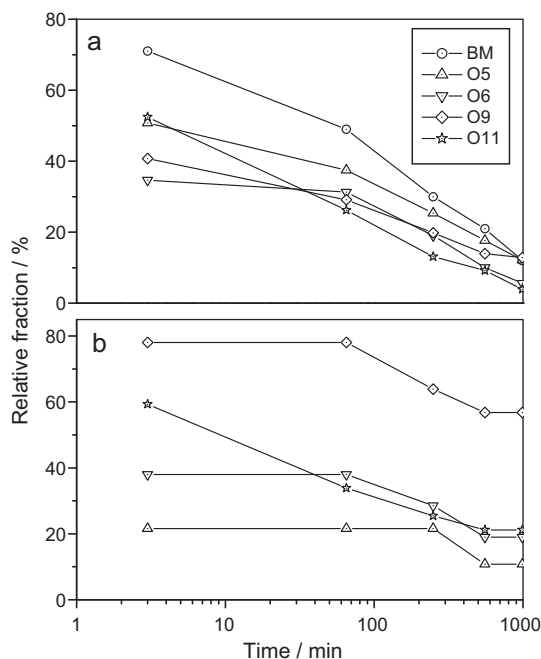


**Fig. 6.** Relative fraction of (a) MgH<sub>2</sub> and (b) Mg–Nb oxides as a function of desorption time at 623 K. The relative fraction is calculated as the ratio of the theoretical and measured wt% in the mixture.

hydride phases might bring to a destabilisation of the desorption reaction due to an increase of the elastic strain in the nanostructured material, leading to an increase of  $T_{dec}$ . In fact, this trend has been estimated for the Ti/TiH<sub>2</sub> reaction [21].

In order to preserve the beneficial effects on the free energy change of desorption reaction due to the presence of nanostructured phases, both small size and elastic strain should be maintained during the hydrogen loading and unloading cycles. Actually, the presence of a higher free energy in the nanostructured with respect to the bulk material develops a driving force for recrystallisation, which promotes a coarsening of the nanostructured phases [20]. This effect could be avoided if a strong activation energy barrier is developed against recrystallisation and grain growth, as recently demonstrated for Mg prepared by inert gas condensation [24]. On the other hand, the dependence of enthalpy and entropy on the excess volume in nanostructured materials seems to suggest a stabilisation of the nanostructure for high values of excess volume [22]. For the Mg/MgH<sub>2</sub> system, this stabilisation has been estimated for  $V_{exc} > 1.3$ , which appears rather high for real systems.

From the experimental results obtained by in situ experiments for both absorption and desorption, it seems clear that a thermodynamic effects on reaction rates should be excluded, because of the observed significant grain growth. On the other hand, even if the nanostructure obtained after ball milling would be preserved during the absorption/desorption cycles, a limited effect should be observed. So, the sharpening of the diffraction peaks of MgH<sub>2</sub> and the limited broadening of the diffraction peaks of Mg, suggest that kinetic effects will take the main role in the reaction rate.

Together with thermodynamic effects, the occurrence of a nanostructured phase might have a significant role on the reaction kinetics, reducing the hydrogen release time in isothermal conditions [2]. In fact, smaller diffusion paths and possible reduction of the activation energy for hydrogenation, promoted by the high density of grain boundaries and interfaces, have to be taken into account in nanostructured materials. In order to estimate the effect of additives on the velocity of dehydrogenation reaction, the MgH<sub>2</sub>

relative fraction, obtained from Rietveld refinement for selected patterns, is reported in Fig. 6a as a function of time for various samples. The MgH<sub>2</sub> relative fraction is calculated as the ratio of the theoretical and measured wt%. Data are reported as a function of the logarithm of time, so that the occurrence of a linear dependence can be associated with a first order reaction, with the slope proportional to the rate constant. It appears clear that the simple ball milling shows a limited effect on the reaction rate. On the contrary, with additives, the desorption reaction appears to be much faster, as suggested by the smaller relative fraction of MgH<sub>2</sub>. Among the various additives, O<sub>11</sub> mixture turns out to have the major effect. In order to identify possible interactions of the additive with the Mg/MgH<sub>2</sub> mixture, the relative fraction of oxide phase is reported in Fig. 6b. At the beginning of the desorption reaction, a significant decrease of the additive is observed, with respect to the as-milled mixtures (Table 1). The reduction of the relative fraction is very strong for O<sub>5</sub> mixture and limited for O<sub>9</sub> mixture. In the case of the O<sub>11</sub> mixture, there is a clear progressive decreasing of the additive content as a function of desorption time, suggesting a significant chemical interaction with the Mg/MgH<sub>2</sub> matrix. This effect can be also related to the interaction of the oxide phase with MgO layer surrounding the Mg/MgH<sub>2</sub> particles [7]. In fact, with respect to the oxidation effects of Mg already observed after ball milling, an increase of the amount of MgO phase is observed during the desorption at 623 K, reaching values up to 40 wt%, likely due to a reaction with residual oxygen in the high temperature XRD chamber.

In all the cases, it turns out that the additives accelerate the desorption reaction and reduce its relative amount during the reaction, suggesting an active role of these phases during the process. This observation is in agreement with suggested “pathway effects” for hydrogen sorption in Mg [7], where a reduction of the oxidation state of Nb from V in Nb<sub>2</sub>O<sub>5</sub> to lower values is suggested. It is worth noting that, for the O<sub>11</sub> mixture a lower oxidation state is already present in the additive, which can facilitate the hydrogen permeation through the MgO layer. In fact, Mg<sub>3</sub>Nb<sub>6</sub>O<sub>11</sub> compound has been shown to be more active for hydrogen absorption at low pressure with respect to Nb(V) based compounds [14–16]. The reversible interaction of hydrogen with Mg<sub>3</sub>Nb<sub>6</sub>O<sub>11</sub> has been tentatively explained in terms of an original structural feature of the solid, i.e., the presence of octahedral niobium clusters in the structure [16]. The octahedral clusters exist in particular structural position in Mg<sub>3</sub>Nb<sub>6</sub>O<sub>11</sub> lattice and are not found in the other oxides here considered. The niobium clusters could act as a sort of insertion site for hydrogen uptake and release, thus explaining the peculiar fast sorption reactions after additions of this compound [16].

## 5. Conclusions

The H<sub>2</sub> sorption reactions in ball milled MgH<sub>2</sub> with addition of Mg–Nb oxides have been studied by in situ XRD analysis. In particular, additions of MgNb<sub>2</sub>O<sub>6</sub>, Mg<sub>4</sub>Nb<sub>2</sub>O<sub>9</sub> and Mg<sub>3</sub>Nb<sub>6</sub>O<sub>11</sub> compounds have been considered, and compared with the addition of Nb<sub>2</sub>O<sub>5</sub> and simple ball milling of MgH<sub>2</sub>. It was observed that the rate of the H<sub>2</sub> desorption reaction at 623 K and of hydrogen absorption at 573 K is significantly accelerated by the presence of additives. Among the various additives considered, Mg<sub>3</sub>Nb<sub>6</sub>O<sub>11</sub> seems to show the best performances for the desorption reaction, whereas a similar behavior was observed for the absorption process. The driving forces for hydrogen absorption and desorption have been calculated on the basis of available thermodynamic databases. It turns out that a faster desorption reaction would be expected on the basis of thermodynamic arguments. The effect of nanostructure on the thermodynamics of hydrogen desorption in MgH<sub>2</sub> has been presented and it has been demonstrated that a very small crystallite size (lower than 3 nm) would be necessary in order to change

significantly the equilibrium temperature of the reactions. So, a reaction mechanism, based on the high mobility of hydrogen in  $Mg_3Nb_6O_{11}$ , has been suggested.

## References

- [1] J. Huot, G. Liang, S. Boily, A. Van Neste, R. Schulz, J. Alloys Compd. 293 (1999) 495.
- [2] R.A. Varin, T. Czujko, Ch. Chiu, Z. Wronski, J. Alloys Compd. 424 (2006) 356.
- [3] J.R. Ares, K.-F. Aguey-Zinsou, T. Klassen, R. Bormann, J. Alloys Compd. 435–435 (2006) 729.
- [4] B. Sakintuna, F. Lamari-Darkrim, M. Hirsher, Int. J. Hydrogen Energy 32 (2007) 1121.
- [5] O. Friedrichs, T. Klassen, J.C. Sánchez-López, R. Bormann, A. Fernandez, Scripta Mater. 54 (2006) 1293.
- [6] K.-F. Aguey-Zinsou, J.R. Ares, T. Klassen, R. Bormann, Int. J. Hydrogen Energy 32 (2007) 2400.
- [7] O. Friedrichs, J.C. Sánchez-López, C. López-Cartes, T. Klassen, R. Bormann, A. Fernandez, J. Phys. Chem. B 110 (2006) 7845.
- [8] N. Hanada, T. Ichikawa, S. Hino, H. Fujii, J. Alloys Compd. 424 (2006) 46.
- [9] V.V. Bhat, A. Rougier, L. Aymard, G.A. Nazri, J.-M. Tarascon, J. Alloys Compd. 460 (2008) 507.
- [10] O. Friedrichs, L. Kolodziejczyk, J.C. Sánchez-López, A. Fernández, L. Lyubanova, D. Zander, U. Köster, K.F. Aguey-Zinsou, T. Klassen, R. Bormann, J. Alloys Compd. 463 (2008) 539.
- [11] M. Dornheim, N. Eigen, G. Barkhordarian, T. Klassen, R. Bormann, Adv. Eng. Mater. 8 (2006) 377.
- [12] A. Borgshulte, U. Bösenberg, G. Barkhordarian, M. Dornheim, R. Bormann, Catal. Today 120 (2007) 262.
- [13] F. Dolci, M. Di Chio, M. Baricco, E. Giamello, J. Mater. Sci. 42 (2007) 7180.
- [14] F. Dolci, M. Di Chio, M. Baricco, E. Giamello, Mater. Res. Bull. 44 (2009) 194.
- [15] F. Dolci, M. Baricco, P.P. Edwards, E. Giamello, Int. J. Hydrogen Energy 33 (2008) 3085.
- [16] M.W. Rahman, S. Livraghi, F. Dolci, M. Baricco, E. Giamello, Int. J. Hydrogen Energy, in press, doi:10.1016/j.ijhydene.2011.01.053.
- [17] T.R. Jensen, A. Andreasen, T. Vegge, J.W. Andreasen, K. Stahl, A.S. Pedersen, M.M. Nielsen, A.M. Molenbroek, F. Besenbacher, Int. J. Hydrogen Energy 31 (2006) 2052.
- [18] L. Lutterotti, S. Matthies, H.-R. Wenk, A.J. Schulz, J. Richardon, J. Appl. Phys. 81 (1997) 594–600. Available from: <http://www.ing.unitn.it/~maud>.
- [19] M.W. Chase Jr., NIST-JANAF thermochemical tables, fourth ed., J. Phys. Chem. Ref. Data, Monogr. 9 (1998) 1.
- [20] V. Bérubé, G. Radtke, M.S. Dresselhaus, G. Chen, Int. J. Energy Res. 31 (2007) 637.
- [21] V. Bérubé, G. Chen, M.S. Dresselhaus, Int. J. Hydrogen Energy 33 (2008) 4122.
- [22] V. Bérubé, M.S. Dresselhaus, G. Chen, Int. J. Hydrogen Energy 34 (2009) 1862.
- [23] R.W.P. Wagemans, J.H. van Lenthe, P. de Jongh, A.J. van Dillen, K.P. de Jong, J. Am. Chem. Soc. 127 (2005) 16675.
- [24] E. Callini, L. Pasquini, E. Piscopiello, A. Montone, M. Vittori Antisari, E. Bonetti, Appl. Phys. Lett. 94 (2009) 221905.
- [25] K.C. Kim, B. Dai, J.K. Johnson, D.S. Sholl, Nanotechnology 20 (2009) 204001.
- [26] A. Baldi, M. Gonzalez-Silveira, V. Palmisano, B. Dam, R. Griessen, Phys. Rev. Lett. 102 (2009) 226102.